Proceedings World Geothermal Congress 2020+1
Reykjavik, Iceland, April - October 2021

Investigation of a Rapid Geothermal Aluminosilicate Scale Formation Mechanism: Preliminary Results of Kinetic Experiments

Claire J NEWTON [1*], Michael C ROWE [1], Sadiq J ZARROUK [2]

[1] School of Environment, The University of Auckland, Private Bag 92019, Auckland, New Zealand

[2]Department of Engineering Science, The University of Auckland, Private Bag 92019, Auckland, New Zealand

*claire.newton@outlook.co.nz

Keywords: Aluminosilicate, scale, silica, aluminium hydroxide, boehmite, kinetic, experiment, colloid, precipitation, reaction hydroxyaluminosilicate, reservoir, reinjection, mitigation, prevention, San Jacinto-Tizate.

ABSTRACT

Amorphous aluminosilicate scales have been observed to form in geothermal pipelines at numerous locations internationally, with examples reported from geothermal fields in Iceland, El Salvador, Nicaragua, New Zealand, Japan, Indonesia, and the Philippines. These scales frequently accumulate at higher rates and temperatures than would be expected for pure amorphous silica scales, resulting in the unexpected fouling of surface infrastructure, and injectivity declines in geothermal brine reinjection wells; both of which present significant problems for the utilisation of geothermal energy. Yet, though this phenomenon has been studied for over 40 years, a mechanism responsible for the formation of aluminosilicate scales has yet to be unequivocally identified. In this work, aluminosilicate colloids were synthesised and captured under controlled conditions during time-constrained aqueous experiments. The rapid formation of aluminosilicate colloids was found to coincide with the supersaturation of aluminium (oxy)hydroxide, producing filterable aluminosilicate colloids within 120 seconds, with the initially Al-rich colloids becoming increasingly Si-rich with reaction time. Aluminosilicate colloids synthesised under neutral to alkaline conditions sequester both Na and K during their earliest formation, with Si/Al, K/Na, and Al/K+Na) mole ratios approaching those of real geothermal scales formed at the San Jacinto-Tizate field study site, as well as others reported in the literature. Similarly, these synthesized colloids demonstrate a near identical $(K/Na)_{[solid]}/(K/Na)_{[brine]}$ enrichment to that of real geothermal aluminosilicate scales. The onset of aluminosilicate formation appears to be independent of aqueous silica concentration, and the saturation state of silica with respect to amorphous silica, although the solution Si/Al mole ratio does influence the stoichiometry of the colloids produced. These latter two features are congruent with a formation mechanism identified for amorphous aluminosilicates formed at low temperatures under acidic conditions within recent hydroxyaluminosilicate (HAS) research. Although these preliminary results require further testing, the successful synthesis of artificial geothermal aluminosilicate colloid analogues demonstrated by this work presents an invaluable opportunity to both better resolve geothermal aluminosilicate-scaling processes, and more rigorously test methods of aluminosilicate scale mitigation and prevention.

1. INTRODUCTION

1.1 Previous research

Aluminosilicate scales, with Si/Al mole ratios typically ranging between 5 and 8, have been found to deposit in the pipes of a number of geothermal power stations internationally (Table 1.1). These scales are frequently formed at much higher temperatures and rates than pure amorphous silica scales (Ichikuni, 1970; Thórhallsson et al., 1975; Arnórsson, 1981; Gallup, 1997; Gallup, 1998; Raymond et al., 2005; Thermochem, 2010), with a diverse range of formation/trigger mechanisms previously proposed to explain their occurrence. The dominant aluminosilicate scale formation mechanisms currently postulated within the geothermal literature are either that Al is sequestered on the surface of pre-polymerised silica (e.g., Yokoyama et al., 1989; Yokoyama, et al., 1993; Gallup, 1997), or that the scales form via direct quasi-equilibrium precipitation of a stoichiometric aluminosilicate phase, such as $NaAlSiO_4$ or $Al_2O_3 \cdot 14\ SiO_2$ (Gallup, 1998; Houston et al., 2008; Mason et al., 2011). Although Al sequestration on silica certainly occurs (Houston et al., 2008; Jolivet et al., 2011), this mechanism does not explain aluminosilicate deposition at significantly higher temperatures and rates than pure amorphous silica scales, as it requires the polymerisation of amorphous silica to occur before this reaction may proceed. Alternatively, the rapid quasi-equilibrium precipitation of stoichiometric aluminosilicate phases may occur at extreme pH, such as $pH \geq 12$, where Al (oxy)hydroxide solubility is very high, as used during the hydrothermal synthesis of zeolite for industrial applications. However, stoichiometrically stable and consistent phases are not observed at micro-scale in amorphous geothermal aluminosilicate scales (Newton, 2018; Newton, 2019). In reality, colloidal aluminosilicates deposited from the same geothermal brine occur over a compositional range, with in-situ compositions of individual particles likely dictated by kinetic factors. Additionally, the stoichiometry and coordination within rapidly precipitated aluminosilicates has been demonstrated to evolve with reaction time (Yokoyama et al, 1999; Doucet et al., 2001b; Yokoyama et al., 2002; Strekopytov and Exley, 2006; Leiviskä et al., 2014; Tokoro et al., 2014; Beardmore et al., 2016). Both of these observations argue against a simple, one step, quasi-equilibrium precipitation reaction, and instead indicate that a more complex and dynamic, kinetic process is likely to be occurring.

In recent years there has been a growing awareness of the important role of rapidly precipitated Al (oxy)hydroxide particles in the formation of aluminosilicate scales in the geothermal energy (Yokoyama et al., 2002) and chemical processing industries (Nishida et al., 2009; Lagref and Haci, 2014). With this kinetic mechanism also recognised as a step during the synthesis of artificial aluminosilicate materials used in various commercial applications (Ryu et al., 2010). Additionally, the incipient nucleation of Al (oxy)hydroxide solids is now well documented as a trigger for the rapid precipitation of amorphous aluminosilicates at lower temperature (Exley and Birchall, 1993; Doucet et al., 2001a; Doucet et al., 2001b; Exley et al., 2002; Strekopytov and Exley, 2006; Exley, 2012; Leiviskä et al., 2014; Tokoro et al., 2014; Beardmore et al., 2016). Although the conditions of high temperature

geothermal brines are markedly different to those found in soil pore fluids and shallow groundwaters, it is very possible that this trigger mechanism may also operate in hot geothermal brines. The solubility of Al with respect to Al (oxy)hydroxide is extremely temperature sensitive over the range of temperatures and pH commonly observed in geothermal fluids as they are extracted from the reservoir and processed through surface infrastructure. For instance, at neutral pH, the solubility of Al, with respect to boehmite, reduces by a factor of almost 90 between 300°C (2.3 ppm) and 100°C (0.027 ppm) [calculated using thermodynamic data from Bénézeth et al. (2001)], with these Al concentrations encompassing those measured in most commercially exploitable geothermal brines (e.g., Yokoyama et al., 1993; Gallup, 1997; Raymond, 2005). The kinetics of Al (oxy)hydroxide precipitation are rapid (Bénézeth et al., 2008). Similarly, the reaction of aqueous silica with nanoscale Al (oxy)hydroxide sols has also been demonstrated to be very quick, even at low temperature (Tokoro et al., 2014). Taken together, these characteristics present a reasonable prima facie case for this mechanism also being potentially responsible for the rapid deposition of aluminosilicate scales from geothermal brines undersaturated with amorphous silica.

1.2 Scaling at the San Jacinto-Tizate project

A case study location is provided by the San Jacinto-Tizate project, Nicaragua, from which aluminosilicate scale has been characterized in two previous reports (Newton et al., 2018; Newton, 2019). Synthetic aluminosilicate materials produced during experiments documented in this work are compared against natural materials obtained from San Jacinto-Tizate, with more detailed information regarding these samples available within these previous reports (Newton et al., 2018; Newton, 2019). A synopsis of operations and scaling at San Jacinto-Tizate is, however, provided below.

Electricity production at San Jacinto-Tizate began in 2005, with the commissioning of two 5 MW_e back pressure turbines, with anomalous, sub silica-saturation, aluminosilicate scaling observed as early as 2010 at the SJ1-1 brine injection wellhead, and decommissioned SJ6-1 reinjection line (Thermochem, 2010). In 2012, two 36 MW_e condensing turbines were commissioned, which utilize steam from several more recently developed high enthalpy geothermal wells. Four of these wells, SJ12-2, SJ12-3, SJ12-4, and SJ12-5, produce fluid with silica concentrations of approximately 700 ppm (total discharge), amongst the highest observed at San Jacinto (Libbey et al., 2017; J. Guidos, pers. comm., 2018). Brine from these wells is discharged via a steam separator (HPS3) into the North Reinjection Line (NRL), and subsequently reinjection well SJ-11-1, and S12-2 since 2018. Since being put into use in 2012, the NRL has experienced rapid aluminosilicate scaling, which was accompanied by significant injectivity decline in SJ11-1 (Escobar and Escalante, 2015; Libbey et al., 2017). In an attempt to combat this scaling, dosing of the geothermal brine with a series of commercial silica dispersant/antiscalant products was tested from mid-2014 through to mid-2016, with none of these agents proving to be fully effective (Escobar and Escalante, 2015). Following this, two organic acids were tested, beginning in November 2016, with both acetic and citric acid proving effective at controlling pure silica polymerisation in the NRL brine (Matus and Guidos, 2017), with acetic acid being finally selected for longer term testing in March 2017. Acid dosing of pad SJ12 brines has been supplemented by dilution with low SSI brine from the southern part of the field, making use of the additional injection capacity provided by SJ11-2 since 2018, the combination of which has reduced brine SSI to 1.0-1.1 (Gamez and Guidos, 2019).

This new injection regime appears to be providing excellent control of both SSI and pure silica polymerization. However, a variety of light pinkish-brown silicate scale continues to be deposited within the NRL (Gamez and Guidos, 2019; Newton, 2019). This light pinkish-brown coloration was found to be correlated with high metal content, particularly Al, within an earlier scaling report prepared by the author (Newton, 2018). Also during this period (2018-2019), the wellhead pressure (WHP) of the SJ11-1 and SJ11-2 injectors has been observed to gradually increase, while injection capacity has declined (J. Guidos, pers. comm., 2019). However, it is not yet known whether this is due to scaling within the injection formation, or an increase in formation pressure due to SJ11-2 coming online.

1.3 Geothermal scaling experiments

Solution experiments were conducted at 80ºC to simulate the earliest stages of aluminosilicate colloid formation, and test whether the supersaturation of gibbsite/boehmite may be responsible for triggering the production of aluminosilicate scales. Solids produced during laboratory experiments are compared against genuine geothermal scales, while the composition of test solution filtrates are used to determine both a reaction mechanism and obtain an understanding of reaction rate. The combination of these data and observations is then used to infer a possible mode of formation of geothermal aluminosilicate scale at San Jacinto-Tizate, and potentially other geothermal fields.

2. METHODS

2.1 Experimental

Geothermal solution experiments were carried out at 80ºC in a polytetrafluoroethylene (PTFE) reaction vessel (Fig. 2.1), with both the reaction vessel and temperature control system (Fig. 2.2) constructed specifically for this study by the author. Conditions of the reacting solutions were changed steadily, with solution samples regularly extracted via a 0.1 μm pore size membrane filter suspended within the test solution. The aim of the sample filtration was to capture a large enough proportion of any solids produced so that precipitation reactions may be detectible via a decline in solute concentration of the filtrates.

These experiments included both silica-supersaturated (SS) and silica-undersaturated (US) runs in the presence of Al, SS with no Al, Al with no silica, and both SS and US experiments carried out at greater Al concentrations (Table 2.2). Additionally, following the observation via FESEM that Na was also incorporated into the rapidly formed aluminosilicate colloids, K was also added to several runs to test whether this element would be favorably incorporated into the formed aluminosilicate colloids, as observed in real-world aluminosilicate scales. Initial test solution Na/K ratios were established at approximately 4.5 (ppm basis), similar to that of the Pad SJ12 geothermal brines (Libbey et al., 2017), and typical of the approximately 2-10 Na/K (ppm basis) range of other geothermal brines (Ichikuni, 1970; Thorhallsson et al., 1975; Yokoyama et al., 1993; Gallup, 1989; Yokoyama et al., 1999; Reyes et al., 2001).

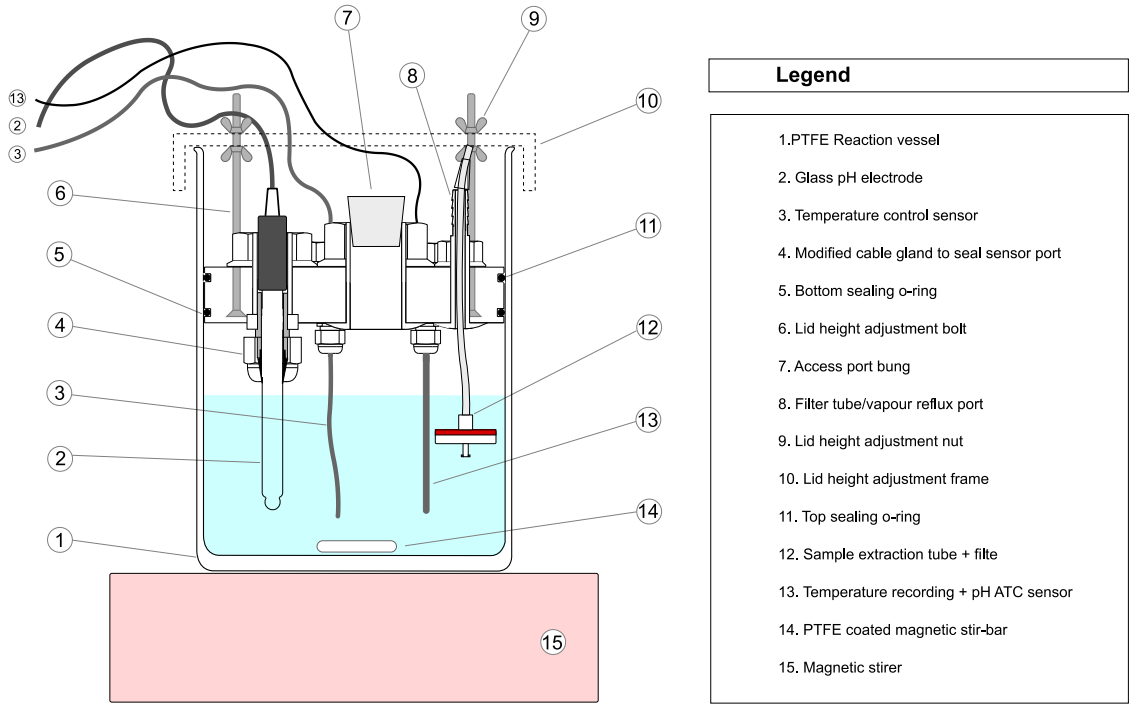

Figure 2.1: Experiment reaction vessel and components.

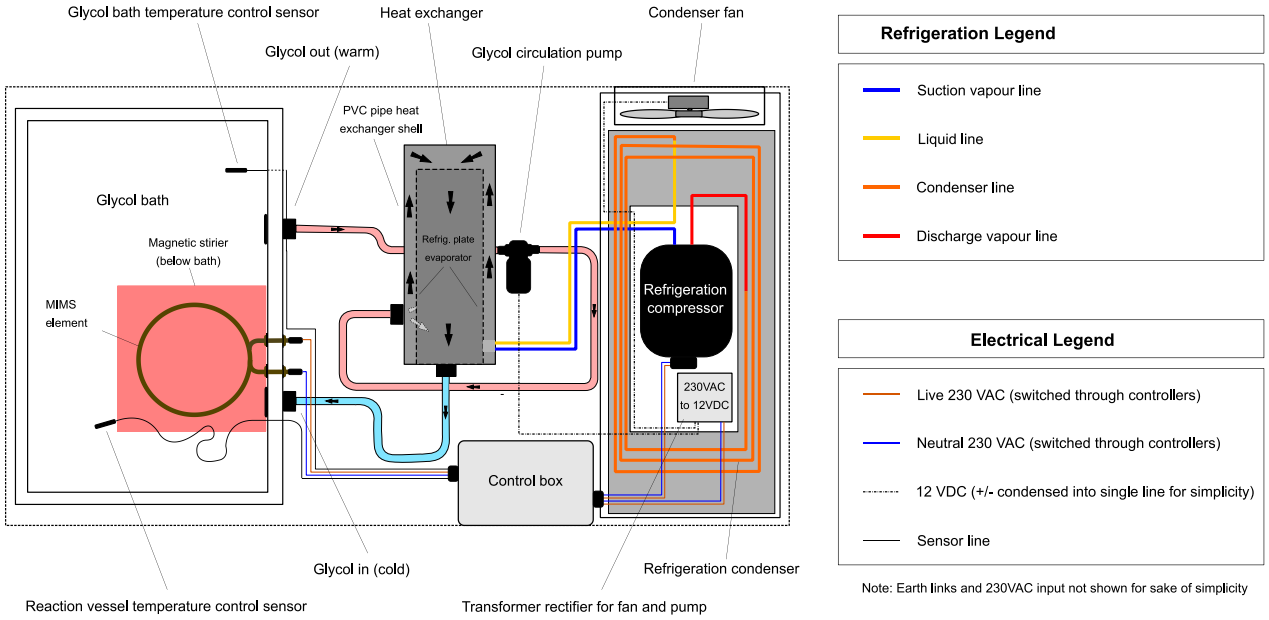

Figure 2.2: Experiment temperature control machine

The saturation of Al (with respect to gibbsite/boehmite) and silica was increased stepwise, from undersaturation to supersaturation from high pH, via pH adjustment. HCl stock solution was added to reduce pH in half-unit increments from an equilibration pH of ~10 to neutral. This made use of the sensitivity of both gibbsite/boehmite and amorphous silica solubility to pH over this pH range (Fig. 2.3), and allowed solubility of both to be altered rapidly with relative precision. At each half-unit pH step, filtered samples were drawn through a 0.1 µm polyethersulfone (PES) membrane filter, followed by turbidity measurements taken using a preheated turbidity tube. The 'equilibration' time of each step was kept constant, with an initial filtered sample and turbidity measurement taken after 2 minutes following pH adjustment, with a second sample and turbidity measurement taken after a further 10 minutes. Solution samples were digested with HNO_3 to ensure homogeneity, and analysed via ICPMS.

Table 2.1: Geothermal experiment design and actual starting solution compositions, given in ppm (actual measured values given in brackets). *Al indicates 'high Al concentration' experiment.

	Experiment code			
Component	80A	80B	80C	80D
SiO_2	240 (280)	380 (410)	380 (400)	0 (0.3)
Al	2 (3)	2 (3)	0 (0.3)	2 (3)
Na	350	460	280	160
Classification	*(US + Al)*	*(SS + Al)*	*(SS)*	*(Al)*

	Experiment code (higher Al experiments)				
Component	80E01	80E02	80E03	80F01	80F02
SiO_2	240 (200)	240 (240)	240 (310)	380 (384)	380 (390)
Al	10 (11)	10 (12)	10 (14)	10 (11)	10 (12)
Na	970	1360	970	1160	1060
K	n/a	230 (200)	230 (220)	n/a	250 (240)
Classification	*(US + *Al)*	*(US + *Al + K)*	*(US + *Al + K)*	*(SS + *Al)*	*(SS + *Al + K)*

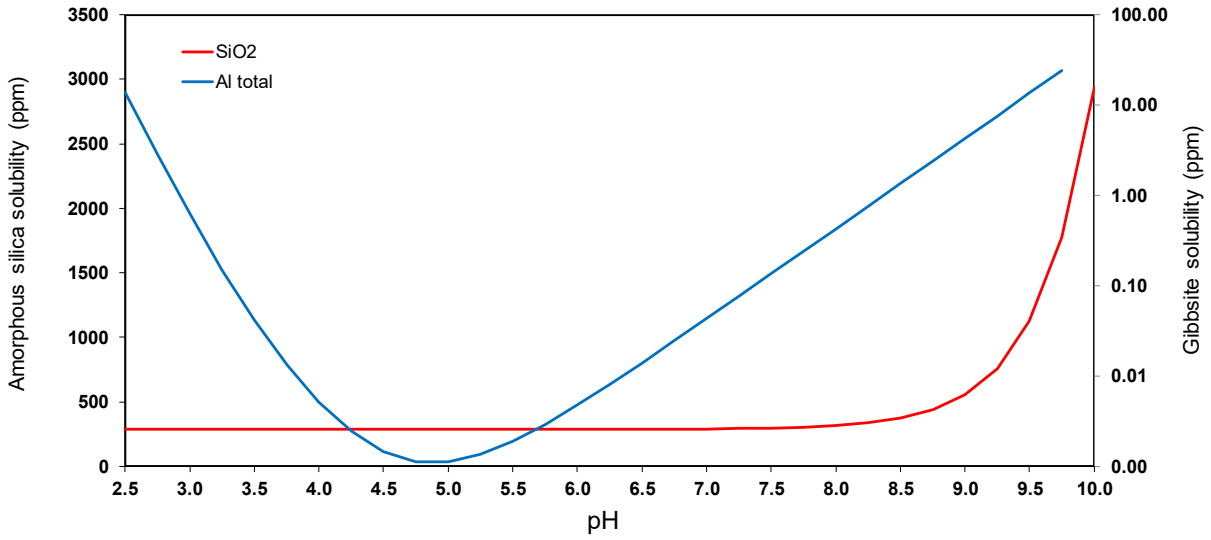

Figure 2.3: pH dependent solubility of amorphous silica and gibbsite at 80°C, calculated via method of Fleming and Crerar (1982), and thermodynamic data from Wesolowski and Palmer (1994) and Bénezeth et al. (2001).

2.2 Material analysis

In-situ micro-chemical analyses and imaging of precipitates captured on filter membranes during geothermal scaling experiments was carried out with a Philips XL30S Field Emission Gun Scanning Electron Microscope (FESEM) equipped with a Si-Li (Lithium drifted) Energy Dispersive Spectrometer (EDS) located in the Research Centre for Surface and Materials Science (RCSMS), University of Auckland, New Zealand.

3. RESULTS AND DISCUSSION

Overall, the onset of synthetic geothermal aluminosilicate formation was found to closely coincide with gibbsite/boehmite saturation. Strong evidence for this was provided by the higher Al concentration versions of the geothermal aluminosilicate series of experiments (Fig. 3.1), although the lower Al concentration experiments were less successful in detecting these reactions via changes in filtrate composition alone (Fig. 3.2). However, changes in solution turbidity coincident with gibbsite/boehmite saturation, and the recovery of aluminosilicate materials from these test solutions, indicate that the precipitation reaction very likely did occur as predicted in these cases. Experiment 80D (Fig. 3.5) (Al only, no silica) demonstrated that gibbsite was able to rapidly precipitate at the Al concentration and conditions of the low Al experiments. Meanwhile, in test solutions containing the same initial concentration of Al (3 ppm), but in the presence of SiO_2 (experiments 80A and 80B) (Fig. 3.2), only sparing amounts of solid material were able to intercepted by the membrane filters.

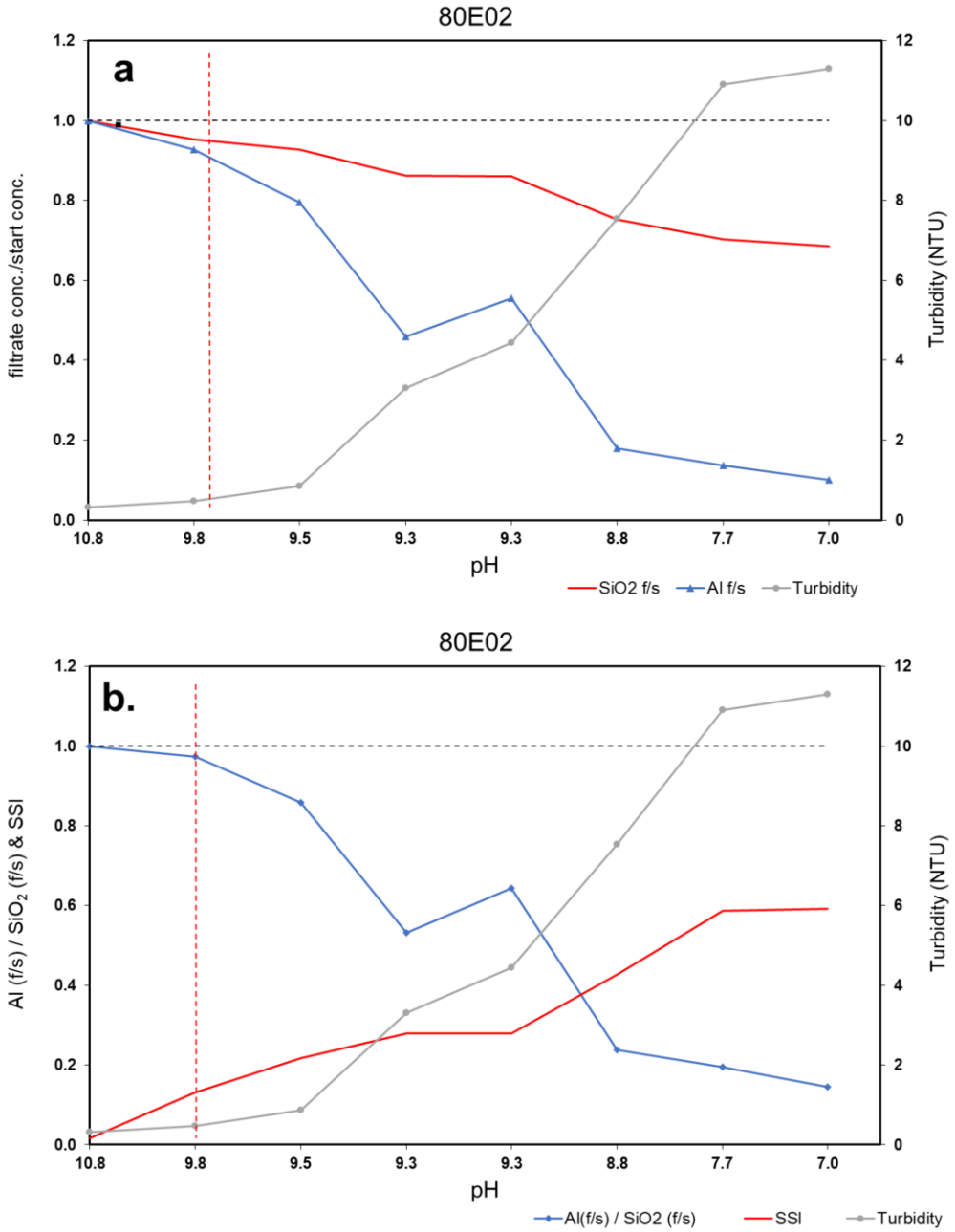

Figure 3.1: High Al experiment 80E02. (a) filtrate Al and SiO_2 concentrations at each pH adjustment step divided by the initial solution concentration (filtrate/start = f/s) for each component, turbidity is also shown. (b) Al f/s, divided SiO_2 f/s, SSI and turbidity are also shown. Areas to the right of the vertical, dashed red line (both charts), exceed gibbsite saturation, while the grey dashed line indicates f/s and SSI = 1.

This was anticipated as being a potential problem because early HAS research indicated that the size of aluminosilicate particles precipitated from alkaline solutions, and consequently the proportion of filterable materials, is very small compared to equivalent solutions free of SiO_2 (Exley and Birchall, 1993).

The saturation state of SiO_2 with respect to amorphous silica is found to have no influence on the triggering of the reaction which produces synthetic geothermal aluminosilicate. However; no reaction was observed to occur prior to the saturation of gibbsite. Unfortunately, no experiment was able to be carried out in the complete absence of Al due to the contamination of the sodium metasilicate (used as a source of aqueous silica in these experiments) with a small, but significant, quantity of Al. Despite this challenge, experiment 80C demonstrated that the supersaturation of amorphous silica was not able to produce filterable colloidal amorphous silica during the approximately 30 minutes for which this material was supersaturated. In contrast to this, both the 80E and 80F series, gibbsite-supersaturated experiments were able to form large quantities of filterable solids (Fig. 3.3) within 120 seconds of gibbsite reaching saturation.

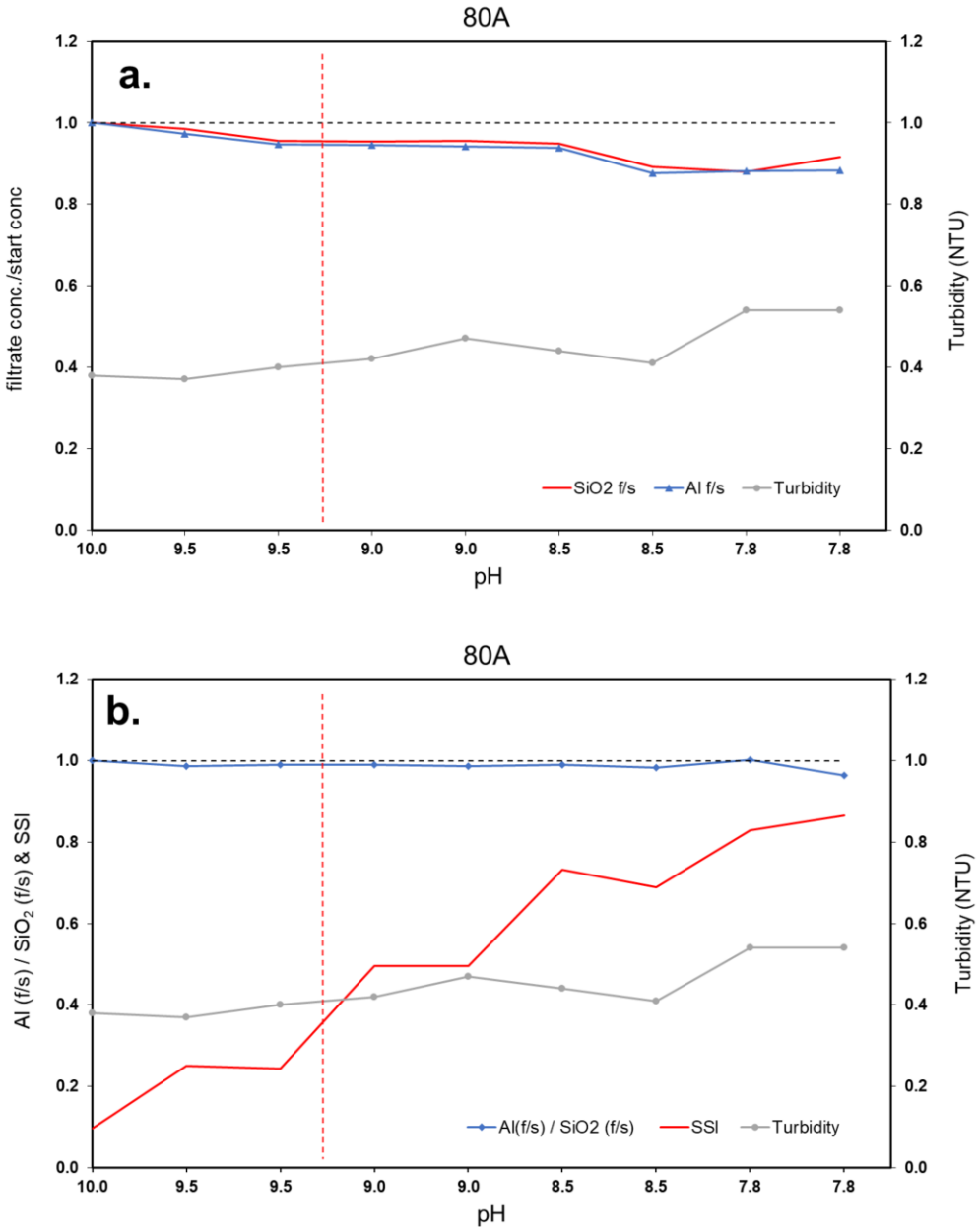

Figure 3.2: High Al experiment 80E02. (a) filtrate Al and SiO_2 concentrations at each pH adjustment step divided by the initial solution concentration (filtrate/start = f/s) for each component, turbidity is also shown. (b) Al f/s, divided SiO_2 f/s, SSI and turbidity are also shown. Areas to the right of the vertical, dashed red line (both charts) exceed gibbsite saturation, while the grey dashed line indicates f/s and SSI = 1.

Aluminosilicate materials achieved Si/Al ratios as high as ~4.1, slightly less than the most Al-rich amorphous aluminosilicate recorded at San Jacinto-Tizate (~4.6 from C-01) (Table 3.1). However, in all other respects, the synthetic aluminosilicate was almost identical in terms of composition. Laboratory synthesised aluminosilicate incorporated alkali elements at a relatively consistent mole ratio with respect to Al, similar to San Jacinto aluminosilicate scales, with average alkali cation/Al mole charge ratios of 0.92 and 0.84, respectively. [K+Na+2Ca-Cl]/Al is given for the geothermal scales, as Ca is present in the natural brine, and is incorporated as a charge-balancing cation within the scales from which they form, likely in competition with Na and K. Meanwhile, Ca was absent from experiment test solutions, so was not able to be incorporated into the synthetic solids, leaving Na and K as the only potential charge-balancing cations available. Similarly $(K/Na)_{[solid]}/(K/Na)_{[brine]}$ enrichment ratios of synthetic aluminosilicate and San Jacinto-Tizate scale were very similar (Table 3.1), averaging 8.2 and 7.4 respectively.

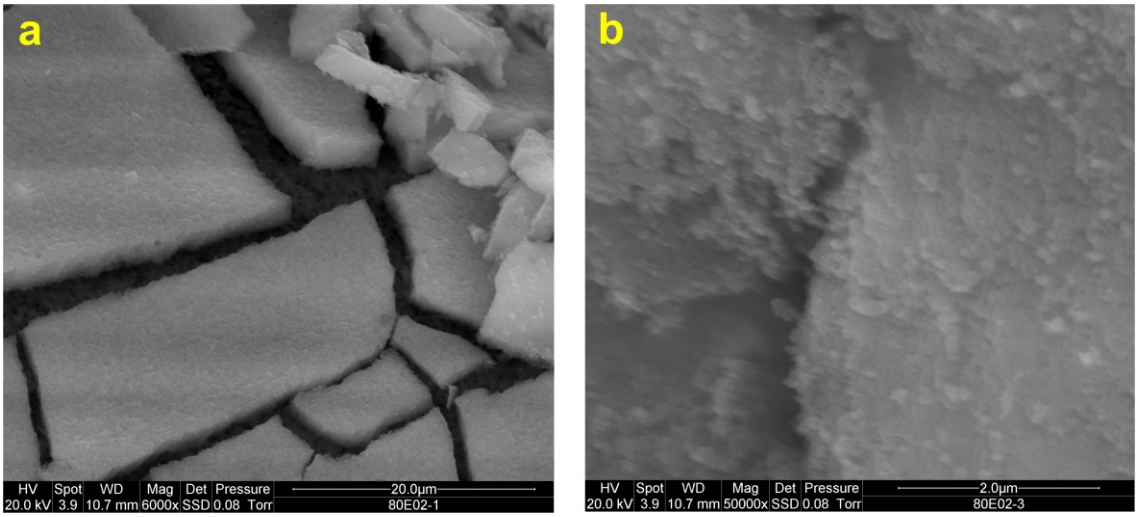

Figure 3.3: FESEM images of 80E02 filter membranes. (a) Filter 1 colloidal aluminosilicate coating, cracks due to drying membrane extraction, average Si/Al mole ratio of filter 1 = 2.15, $(K/Na)_{[solid]}/(K/Na)_{[brine]]} = 3.46$. (b) Filter 3 colloidal aluminosilicate, average Si/Al mole ratio of filter 3 = 2.93, average $(K/Na)_{[solid]}/(K/Na)_{[brine]} = 7.19$.

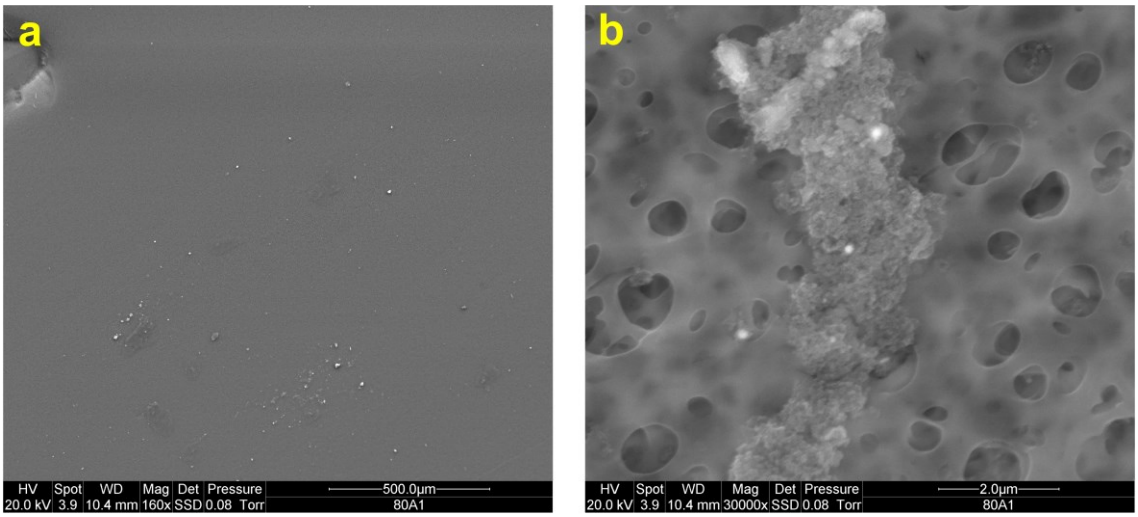

Figure 3.4: FESEM images of 80A filter membranes. (a) low magnification view of membrane surface, some isolated aggregations of colloids are visible, Si/Al mole ratio of whole image area = 1.93 (b) in-situ colloid aggregation, note the size of membrane filter pores compared to the individual colloidal components of the aggregation, colloid Si/Al mole ratio = 3.19.

Despite the significant differences in test solution composition within the 80°C series of geothermal experiments, the solids produced are all of relatively similar composition (with the exception of the SiO_2-free 80D experiment). The most striking differences instead being the variability in the volume of precipitates recovered on the membrane filters, and the degree to which test solution turbidity changed. Also intriguing, is that the Si/Al mole ratio of the synthetic aluminosilicates recovered seems to be more dependent on the bulk concentration of SiO_2, rather than the relative concentration of SiO_2 and Al in the test solutions. For example, the Si/Al mole ratios of the synthetic geothermal aluminosilicate produced by the high SiO_2 (~400 ppm) 80B, 80C, 80F01, and 80F02 experiments (Table 2.2) are all relatively similar, at around 3 or above (Table 3.1). This is in spite of the test solution Al/SiO_2 ratios of these experiments varying by a factor of over 40. Meanwhile the Si/Al mole ratios of the solids produced by the lower SiO_2, 80A (280 ppm) and 80E01 (200 ppm) experiments (Table 2.2) were slightly lower, at closer to 2 (Table 3.1). Again, this in spite of the variation in the Al/ SiO_2 ratios of the starting solutions also being significant, with the ratios of this latter group varying by a factor of just over 5. In contrast, experiment 80E03 experiment (310 ppm SiO_2) produced material closer to that of the higher SiO_2 experiments. The K spiked 80E02 test solution (240 ppm SiO_2) also demonstrates that the composition of the synthetic aluminosilicate solids evolves with reaction time, with average Si/Al mole ratios of materials captured on each membrane filter increasing steadily with each filter change (Table 3.1).

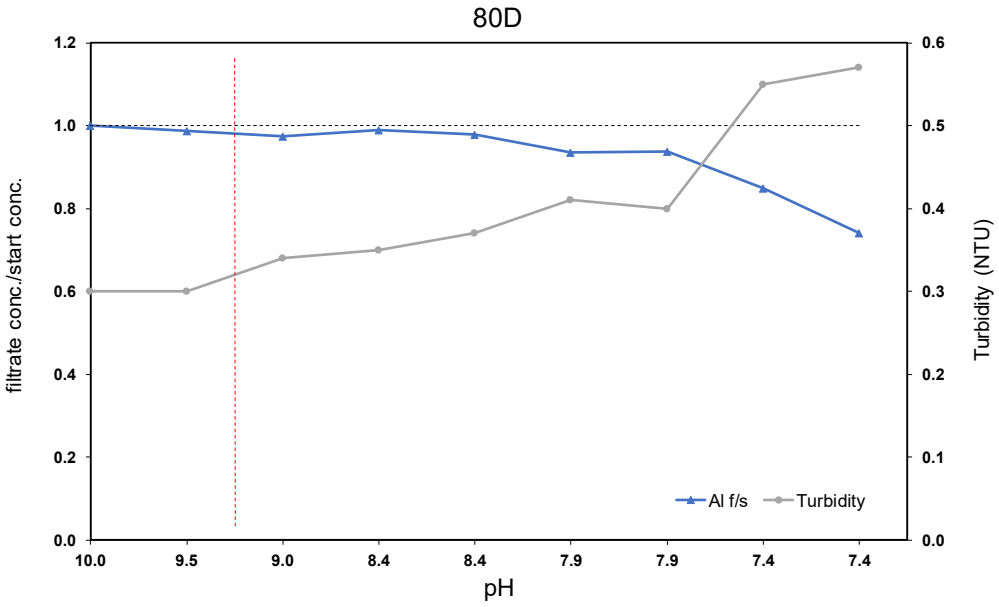

Figure 3.5: 80D, Al only (silica absent). Note the steadily increasing turbidity immediately following boehmite saturation. Filtrate Al concentration at each pH adjustment step divided by the average of the first two measurements (filtrate/start = f/s), turbidity is also shown. Areas to the right of the vertical, dashed red line (both charts) exceed gibbsite saturation, while the black dashed line indicates f/s = 1.

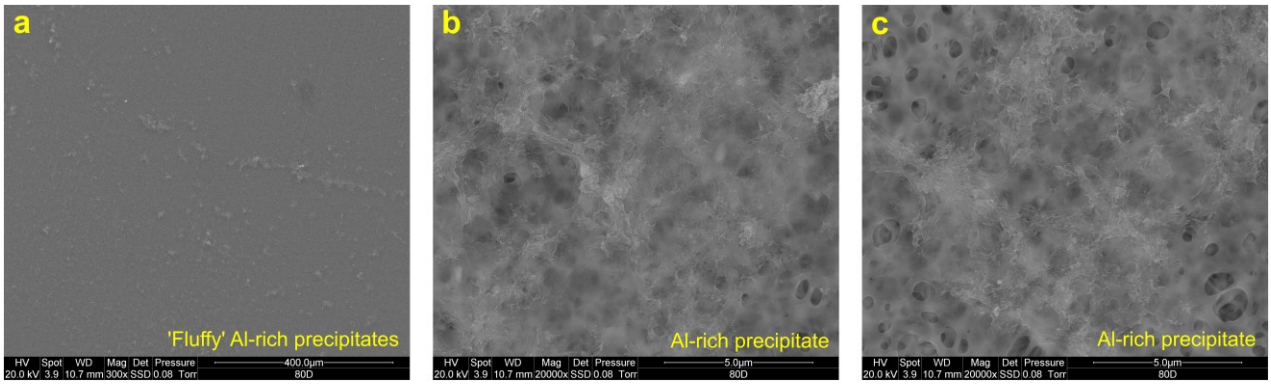

Figure 3.6 FESEM images of experiment 80D filter membrane. (a) Low magnification view of the filter surface, precipitates appear fluffy at this level of magnification. (b) and (c) in-situ Al-rich precipitates. These are somewhat web-like at higher magnification.

This relative similarity in recovered material between various experiments, despite the significant differences in Al concentration and Al/ SiO_2 ratio of the test solutions, is very useful for understanding the reaction processes for solutions for which less colloidal material was able to be intercepted by the membrane filters. Experiment 80D indicates that Al hydroxide precipitates rapidly when Al becomes supersaturated with respect to gibbsite. This reaction was initially detected via an increase in test solution turbidity at the point of gibbsite saturation, which was subsequently accompanied by a reduction in Al concentration in the sample filtrates, approximately one pH unit later at step 5a (pH 7.9). The turbidity measurement was taken only few minutes after gibbsite saturation was exceeded, which is indicative of the rapidity of this precipitation reaction. Enough material was intercepted by the 80D membrane filter (Fig. 3.6) as to induce minor cavitation of the filtrate during sample filtration and extraction, due to an increase in pressure differential across the membrane, from step 5a (pH 7.9); where a reduction in filtrate concentration is initially noted. Meanwhile, in test solutions containing the same initial concentration of Al (3 ppm), but in the presence of SiO_2 (experiments 80A and 80B), only sparing amounts of solid material were able to intercepted by the membrane filters.

Despite the ambiguous results of solutions 80A and 80B, the recovery of synthetic geothermal aluminosilicate, along with the increases in turbidity observed during the course of these experiments were, however, encouraging with regard to the predicted aluminosilicate reaction occurring. In contrast to the 80A&B experiments, the results of the 80E and 80F series of experiments, with starting Al concentrations of ~12 ppm, were dramatic.

Table 3.1: Comparison of geothermal scales (Newton, 2019) with solid materials produced during geothermal experiments. Geothermal scale K enrichment over Na based on San Jacinto-Tizate well discharge chemistry, enthalpy, and mass flow data from Libbey et al., 2017. K enrichment over Na calculations for synthetic geothermal aluminosilicates are based on the composition of their parental test solutions. Si/Al, [K+Na-Cl]/Al, [K+Na+Ca-Cl]/Al are given on a mole basis. $(K/Na)_{[solid]}/(K/Na)_{[brine]}$ are calculated on a mass (mg/kg water) basis. The Large Area High Value (LAHV) results comprise some individual high-Si/Al, full-frame EDS measurements obtained from large areas of experiment filter membranes.

Geothermal experiments			
Sample	Si/Al	[K+Na-Cl]/Al	$(K/Na)_{[sample]}/(K/Na)_{[brine]}$
80A (large area)	1.93	n/a	n/a
80B (large area)	2.89	n/a	n/a
80C (large area)	3.71	n/a	n/a
80E01 F1 (average)	2.15	1.01	n/a
80E01 F2 (average)	2.24	0.87	n/a
80E02 F1 (average)	2.15	0.87	3.46
80E02 F2 (average)	2.44	0.87	3.64
80E02 F3 (average)	2.93	0.71	7.19
80E03 (average)	2.77	0.80	6.22
80F01 F1 (average)	2.70	0.87	n/a
80F01 F2 (average)	2.82	0.76	n/a
80F02 F1 (average)	2.80	0.87	8.05
80F02 F2 (average)	2.88	0.74	5.94
Overall average	2.65	0.84	5.75
80E02 F3 (LAHV) #1	2.96	0.71	7.38
80E02 F3 (LAHV) #2	2.96	0.70	7.53
80F02 F2 (LAHV) #1	3.17	0.84	8.66
80F02 F2 (LAHV) #2	4.08	0.71	5.92
LAHV average	3.29	0.74	7.37

Geothermal scales			
Sample	Si/Al	[K+Na+2Ca-Cl]/Al	$(K/Na)_{[sample]}/(K/Na)_{[brine]}$
RNP #1	5.56	0.83	7.19
RNP #2	5.11	0.87	4.46
RNP #3	6.75	0.80	8.31
RNP #4	5.47	0.97	10.87
RNP average	5.72	0.87	7.71
S1B #1	5.80	0.86	8.51
S1B #2	6.45	1.01	9.74
S1B #3	5.22	1.01	5.41
S1B #4	7.21	0.85	10.04
S1B average	6.17	0.93	8.42
C-01 #1	4.88	0.80	5.20
C-01 #2	4.63	0.82	9.49
C-01 #3	4.94	0.83	5.64
C-01 #4	4.74	0.89	13.19
C-01 average	4.80	0.84	8.38
Overall average	5.56	0.88	8.17

All 80E and 80F series test solutions displayed significant increases in turbidity coinciding precisely with the saturation of gibbsite. Additionally, all of the 80E and 80F series of experiments (with the exception of experiment 80F02) also show reductions in Al ± SiO_2 concentration and Al/ SiO_2 ratio in the sample filtrates at this same pH adjustment step, or the one immediately following.

Rapidly formed synthetic geothermal aluminosilicates also appear to sequester alkali elements as a part of the earliest stages of their formation, with K favored over Na, and the $(K/Na)_{[solid]}/(K/Na)_{[brine]}$ ratio of the aluminosilicate also appearing to increase with time. This process may explain the $(K/Na)_{[solid]}/(K/Na)_{[brine]}$ enrichment ratios of the Pad SJ12 steam line scales at San Jacinto-Tizate (Newton, 2019). These scales do not have access to the bulk brine from which to sequester alkali elements or Al, and these elements are not fractionated into the steam component of the geothermal fluid. Some fine brine droplets are entrained within the steam as it passes through the steam separator, however (Zarrouk and Purnanto, 2015), though the simple drying out of brine droplets impacting the pipe wall would most likely produce a solid of the same, or very similar K/Na, Ca/Na, and Al/Si stoichiometry to the parental brine. Alternatively, a rapidly formed aluminosilicate colloid, produced in the geothermal brine upstream of HPS3, which then became entrained in the steam within a brine droplet, would indeed be able to produce an aluminosilicate scale with the same K/Na, Ca/Na, and Al/Si enrichment ratios as observed in the Pad SJ12 steam line scales (Newton, 2019).

4. CONCLUSION

The onset of synthetic aluminosilicate formation was found to be independent of aqueous silica concentration, and the saturation state of brine with respect to amorphous silica, although the solution Si/Al mole ratio does influence the final stoichiometry of the colloids produced. The Si/Al mole ratio of synthetic aluminosilicate produced from the individual test solutions was also observed to increase with reaction time for experiments in which multiple membrane filters were used. These features are consistent with those identified during the formation of hydroxyaluminosilicates (HAS) at low temperatures under acidic conditions (Exley and Birchall, 1993; Doucet et al., 2001a; Doucet et al., 2001b; Exley et al., 2002; Strekopytov and Exley, 2006; Exley, 2012; Leiviskä et al., 2014). The concentration of K in the synthetic solids was also observed to increase relative to Na with reaction time, in a similar fashion to Si/Al. These observations indicate that the reaction is unlikely to be a classic equilibrium precipitation-style reaction, and rather a more complicated kinetically governed multi-step sequence.

Aluminosilicate colloids synthesized under neutral to alkaline conditions sequester both Na and K during their earliest formation, with Si/Al, K/Na, and Al/K+Na) mole ratios approaching those of real geothermal scales formed at the San Jacinto-Tizate field study site, as well as others reported in the literature (Thórhallsson et al., 1975; Gallup, 1998; Yokoyama et al., 1993; Yokoyama et al., 1999). Similarly, these synthesized colloids demonstrate a near identical $(K/Na)_{[solid]}/(K/Na)_{[brine]}$ enrichment to that of real geothermal aluminosilicate scales. Taken together, these results indicate that production of geothermal aluminosilicate scales may be triggered by the saturation of Al with respect to boehmite in geothermal brines. Whether this mechanism represents the dominant pathway by which geothermal aluminosilicate scales are produced remains to be conclusively demonstrated. However, the reaction studied is able to replicate several key characteristics of the natural reaction, and the materials produced by it. Although these preliminary results require further testing via more sensitive methods, the successful synthesis of artificial geothermal aluminosilicate colloid analogues demonstrated by this work presents an invaluable opportunity to both better resolve geothermal aluminosilicate scaling processes, and more rigorously test methods of aluminosilicate scale mitigation and prevention.

REFERENCES

Arnórsson, S. 1981.: Mineral deposition from Icelandic geothermal waters: environmental and utilization problems. *Journal of petroleum Technology*, **33**(01), (1981), 181-187.

Beardmore, J., Lopez, X., Mujika, J.I. and Exley, C.: What is the mechanism of formation of hydroxyaluminosilicates? *Scientific reports*, **6**, (2016), 30913.

Bénézeth, P., Palmer, D.A. and Wesolowski, D.J.: Aqueous high-temperature solubility studies. II. The solubility of boehmite at 0.03 m ionic strength as a function of temperature and pH as determined by in situ measurements. *Geochimica et Cosmochimica Acta*, **65**(13), (2001), 2097-2111.

Bénézeth, P., Palmer, D.A. and Wesolowski, D.J.: Dissolution/precipitation kinetics of boehmite and gibbsite: Application of a pH-relaxation technique to study near-equilibrium rates. *Geochimica et Cosmochimica Acta*, **72**(10), (2008), 2429-2453.

Doucet, F.J., Rotov, M.E. and Exley, C.: Direct and indirect identification of the formation of hydroxyaluminosilicates in acidic solutions. *Journal of inorganic biochemistry*, **87**(1-2), (2001a), 71-79.

Doucet, F.J., Schneider, C., Bones, S.J., Kretchmer, A., Moss, I., Tekely, P. and Exley, C.: The formation of hydroxyaluminosilicates of geochemical and biological significance. *Geochimica et Cosmochimica Acta*, **65**(15), (2001b), 2461-2467.

Escobar, B., Escalante, J.C.: Silica scaling control program SJ12 pad inhibitor performance history: A summary of testing and findings. Polaris Energy Nicaragua S.A. *Unpublished report*, (2015).

Exley, C. and Birchall, J.D.: A mechanism of hydroxyaluminosilicate formation. *Polyhedron*, **12**(9), (1993), 1007-1017.

Exley, C., Schneider, C. and Doucet, F.J.: The reaction of aluminium with silicic acid in acidic solution: an important mechanism in controlling the biological availability of aluminium?. *Coordination Chemistry Reviews*, **228**(2), (2002), 127-135.

Exley, C.: Reflections upon and recent insight into the mechanism of formation of hydroxyaluminosilicates and the therapeutic potential of silicic acid. *Coordination Chemistry Reviews*, **256**(1-2), (2012), 82-88.

Fleming, B.A. and Crerar, D.A.: Silicic acid ionization and calculation of silica solubility at elevated temperature and pH application to geothermal fluid processing and reinjection. *Geothermics*, **11**(1), (1982), 15-29.

Gallup, D.L.: Iron silicate scale formation and inhibition at the Salton Sea geothermal field. *Geothermics*, **18**(1-2), (1989), 97-103.

Gallup, D.L.: Aluminum silicate scale formation and inhibition: scale characterization and laboratory experiments. *Geothermics,* **26**(4), (1997), 483-499.

Gamez, I. and Guidos, J.A.: Silica Scaling Control Program in North Reinjection Line, 2018. *Unpublished report*, (2019).

Gallup, D.L.: Aluminum silicate scale formation and inhibition (2): scale solubilities and laboratory and field inhibition tests. *Geothermic*s, **27**(4), (1998), 485-501.

Ichikuni, M.: Incorporation of aluminium and iron into siliceous sinters. *Chemical Geology*, **6**, (1970), 273-279.

Leiviskä, T., Rämö, J., Lanzani, G., Huhtakangas, S., Laasonen, K. and Pehkonen, S.O.: Quasi-quantitative determination of elemental relationships and surface properties in aqueous aluminium-silicon systems. *Journal of Water Process Engineering*, **1**, (2014), 54-63.

Libbey, R., Lovelock, B., Ussher, G.: San Jacinto-Tizate draft conceptual model update, ZP00955-RPT-DR-045. Jacobs New Zealand Limited. *Unpublished report*, (2017).

Matus, I., Guidos, H.: Acid treatment test to prevent Silica deposition, North Reinjection Line: Final Report. Polaris Energy Nicaragua S.A. *Unpublished report*, (2017).

Newton, C.J., Zarrouk, S.J., Lawless, J., Rowe, M.C., Guidos, J.A., Brown, K.A.: Aluminium-Rich Silica Scaling: San Jacinto-Tizate Geothermal Energy Project, Nicaragua. *Proceedings,* 40th New Zealand Geothermal Worshop, Wairakei, New Zealand (2018).

Newton, C.J.: Interaction of Aluminium with Silica in Geo-fluids: Investigation of a Proposed Compositional Control Mechanism of Natural Waters and Aluminosilicate Precipitation Reactions in Aqueous Systems. *MSc dissertation*, University of Auckland, New Zealand. (2019).

Nishida, I., Shimada, Y., Saito, T., Okaue, Y. and Yokoyama, T.: Effect of aluminum on the deposition of silica scales in cooling water systems. *Journal of colloid and interface science*, **335**(1), (2009), 18-23.

Raymond, J., Williams-Jones, A.E. and Clark, J.R.: Mineralization associated with scale and altered rock and pipe fragments from the Berlin geothermal field, El Salvador; implications for metal transport in natural systems. *Journal of Volcanology and Geothermal Research*, **145**(1-2), (2005), 81-96.

Strekopytov, S., Jarry, E. and Exley, C.: Further insight into the mechanism of formation of hydroxyaluminosilicates. *Polyhedron*, **25**(17), (2006), 3399-3404.

Thórhallsson, S., Ragnars, K., Arnórsson, S. and Kristmannsdóttir, H.: Rapid scaling of silica in two district heating systems. *Proceedings,* 2nd United Nations Symposium on the Development and Use of Geothermal Resources, San Fransico, CA (1975).

Tokoro, C., Suzuki, S., Haraguchi, D. and Izawa, S.: Silicate removal in aluminum hydroxide co-precipitation process. *Materials*, **7**(2), (2014), 1084-1096.

Wesolowski, D.J. and Palmer, D.A.: Aluminum speciation and equilibria in aqueous solution: V. Gibbsite solubility at 50 C and pH 3–9 in 0.1 molal NaCl solutions (a general model for aluminum speciation; analytical methods). *Geochimica et Cosmochimica Acta*, **58**(14), (1994), 2947-2969.

Yokoyama, T., Takahashi, Y., Yamanaka, C. and Tarutani, T.: Effect of aluminium on the polymerization silicic acid in aqueous solution and the deposition of silica of silica. *Geothermics*, **18**(1-2), (1989), 321-326.

Yokoyama, T., Sato, Y., Maeda, Y., Tarutani, T. and Itoi, R.: Siliceous deposits formed from geothermal water I. The major constituents and the existing states of iron and aluminium. *Geochemical Journal*, **27**(6), (1993), 375-384.

Yokoyama, T., Sato, Y., Nakai, M., Sunahara, K. and Itoi, R.: Siliceous deposits formed from geothermal water in Kyushu, Japan: II. Distribution and state of aluminum along the growth direction of the deposits. *Geochemical journal*, **33**(1), (1999), 13-18.

Yokoyama, T., Ueda, A., Kato, K., Mogi, K. and Matsuo, S.: A study of the alumina–silica gel adsorbent for the removal of silicic acid from geothermal water: increase in adsorption capacity of the adsorbent due to formation of amorphous aluminosilicate by adsorption of silicic acid. *Journal of colloid and interface science*, **252**(1), (2002), 1-5.

Zarrouk, S.J. and Purnanto, M.H.: Geothermal steam-water separators: Design overview. *Geothermics*, **53**, (2015), 236-254.